THE EFFECTS OF RESIDUAL STRESS AND HAZ ON FATIGUE CRACK GROWTH IN MIG WELDED 2024 AND 7150 ALUMINIUM

J. Lin*, S. Ganguly**, L. Edwards**, P.E. Irving*

Abstract: The effect of weld residual stress, and hardness profile on fatigue crack propagation in MIG welded 2024 and 7150 aluminium joints was studied. Residual stress fields in the weld were measured using neutron diffraction. Tests were performed using a range of mean stresses and on different starting defect shapes. It was found that fatigue crack propagation in weld metal and HAZ is influenced by crack morphology and also the distribution of residual stress and hardness. Control of these parameters will optimise damage tolerance capability in welded safety critical structures.

INTRODUCTION

High strength aluminium alloys such as 2XXX and 7XXX series until recently have not been regarded as weldable. Welding of aluminium aircraft structures in which these alloys are extensively used has not been a manufacturing option. Recent developments in weld process control [1, 2] together with the advent of novel welding processes such as friction stir welding [3, 4] has permitted high quality welds to be made in these alloys. Even in traditional aluminium weld processes such as Metal Inert Gas (MIG), high integrity welds with good mechanical properties can be made [5]. This raises the possibility of aircraft fabrication using welding, with the cost savings that elimination of riveting would confer.

The fatigue initiation and fatigue crack growth properties of welds in weldable aluminium alloys such as 5XXX and 6XXX series have been extensively documented in previous work [6, 7], and it has been established that residual stresses arising from the weld process exert a powerful and dominating influence on fatigue crack growth rates[8, 9]. As civil aircraft structures are certified using damage tolerance calculations based on fatigue crack growth, these observations require extension to the 2XXX and 7XXX alloys and weld processes suitable for aircraft applications. The advent of advanced neutron and synchrotron diffraction techniques allows for the first time detailed quantitative non-destructive

*   Damage Tolerance Group, SIMS, Cranfield University, Bedfordshire, UK, MK43 0AL

**   Structural Integrity, Department of Materials Engineering, The Open University, Milton Keynes, UK, MK7 6AA

characterisation of residual stresses distribution in welds, and permits correlation of crack growth rate changes across the weld with changes in residual stress [10, 11].

In the present work, the effect of mean stress, residual stress and HAZ hardness on fatigue crack propagation in MIG welded 2024-T351 and 7150-T651 aluminium alloys has been studied. Detailed profiles of weld residual stresses have been made using neutron diffraction techniques, and these have been related to measured crack growth rates.

EXPERIMENTAL

Double pass MIG welded 2024 and 7150 aluminium plates were manufactured using the process described in Thomas [5]. The plates were welded along their long edge with the weld direction parallel to the longitudinal orientation. For 2024-T351, the welded plates were 500(L) X 300(W) X 12(T) mm, welded with 2319 filler. For 7150, the welded plates were 12.7 mm thick, and were welded in W51 heat treatment state with 5039 filler wire. After welding, 7150 plates were heat treated to T651 temper using a dual stage heat treatment.

Dog-bone coupon samples, 7 mm thick, (Figure 1), were machined from the plates. To minimise distortion during machining, plates were surface skimmed 0.25 mm at each cut, alternating top and bottom surfaces. 0.1 mm was removed in the last cut. Semi-circular surface flaws of 1 mm nominal radius were placed at the centre of the weld line using Electric Discharge Machining (EDM). On other samples, through thickness EDM flaws, 1.7 mm long, and of constant length through the thickness (shown in figure 1) were placed at the centre of the weld. Cracks from surface defects will propagate for some distance entirely within the weld metal, whereas cracks from the through thickness defects will propagate in both weld metal and HAZ.

Hardness traverses perpendicular to the weld were made using a micro hardness indenter using a load of 100g to ASTM E92-82 (1989). Transverse tensile tests were performed on the welds to ASTM E 8M (1997). 3D residual stress distributions in the 12.7 mm plates and 7mm coupons were measured using neutron diffraction techniques described in Stelmukh et al.[10], Stelmukh and Edwards[11].

A 250 kN computer controlled mechanical test machine was used to perform constant load amplitude and constant ΔK fatigue crack propagation tests. A Direct Current Potential Difference (DCPD) system calibrated with a travelling microscope was used to monitor crack growth. For the samples with part through cracks, the surface crack length was calculated with the Roe-Coffin Solution (Van Stone and Richardson [12], Gangloff et al.[13]). Stress intensity factor values were calculated using the Newman and Raju expression [14,15]. For samples with a central through crack, crack lengths were calculated using techniques advocated in ASTM E647.

Tests were performed at *R* values of 0.1 (0.05 for 7150) and 0.6. Additionally for 2024 welds, tests were performed at $R = 0.3$. The constant ΔK tests were performed at a *R* ratio of 0.1 using an in-house computer program to control the testing machine and adjust the load. In all tests, the applied value of constant ΔK was $6.0\,MPa\sqrt{m}$. The resolution on crack length was 0.08 mm and the accuracy with which ΔK was maintained constant was better than 1%.

RESULTS

Table 1 shows typical values of transverse tensile properties for the welded samples. The 0.2% proof strength of welded 2024 is 97% of parent metal, and that of welded 7150 is 64% of parent metal. Ductility of both was about 25% of the original.

Figure 2 shows constant amplitude data for fatigue crack growth from surface flaws. These diagrams represent crack growth behaviour up to a distance of 8 to 10 mm from the weld centre line. Crack growth rates in the fusion zone and in 4 to 7 mm of the HAZ are represented. For 2024 welds, there is little effect of *R* ratio on fatigue crack growth over much of the range studied, although an increased effect can be observed when ΔK is near the threshold. For MIG welded 7150, an increased effect of *R* ratio on fatigue crack growth can be observed. The data for 7150 is much more irregular than for 2024, with significant changes in gradient as the crack grows. This implies that the microstructure and residual stresses in different positions in the weld strongly affect crack growth rates. Also shown in figure 2 is parent metal crack growth data. For 2024, the weld data is considerably faster than the solid line marking the mean parent metal data, but still are within the dotted 95% limit of scatter line. For 7150, the weld data is similar to that of parent metal at $R = 0.05$.

Figure 3 shows a comparison of crack growth rates in the surface cracks with those measured on a through crack. Faster crack growth rates for both alloys were found in data from the through cracks although bigger differences (between 3 and 5 times) were found in 7150 welds. Through cracks in 7150 samples grew faster than ones in 2024 by a factor of three. Figure 4 shows SEM pictures of the fracture surface at the boundary of the fusion and HAZ of part through crack samples for both alloys. A lot of sub-cracks in the main fracture surface can be found in the HAZ part of the fracture. The number of sub-cracks in 7150 welds is much greater than the number found in 2024 welds.

Figure 5 shows the hardness and longitudinal residual stress profiles for one side of the welds. The individual data points for residual stress shown in figure 5 have been derived from the original detailed 3D distribution by averaging all data points at a specified distance from the weld centreline. Thus these points are an average value of the stress distribution in the through thickness direction. The volume element for

the stress values is 2 X 2 mm, and the uncertainty in stress is ±10 MPa. In 12.7mm plates, the peak value of longitudinal stress, averaged through the thickness, was 294 MPa. In 7mm thick coupon samples it was reduced to 210 MPa.

Hardness values were measured at the middle thickness section. For 2024 welds, the lowest hardness of less than 110 HV is at the centreline of the weld, in the fusion zone, and the peak hardness of about 160 HV is 2.5 mm from the centreline, at the fusion zone/HAZ boundary. The hardness declines again further into the HAZ**.** The hardness profile of the 7150 welds is similar, but the fusion zone is ~20-30 HV harder, and the peak is between 4-8 mm from the centreline. The decline in hardness in the HAZ is more pronounced, with the lowest hardness of 120 HV at 11 mm. Residual stresses are similar in the two materials, but of different profile. Both profiles have low to moderate values of residual stress on the weld centreline, and a peak some distance away, before declining to near zero at 25-30 mm from the centreline. The stress value at 2024 weld centreline is 90 MPa, increasing to a peak of 220 MPa located at 11-12 mm from the centreline. At the 7150 weld centreline the value of stress is 50 MPa, with a peak of 200 MPa located 5-6 mm from the centreline.

Figure 6 shows the variation of crack growth rate with crack length during the constant $\Delta K = 6$ $MPa\sqrt{m}$ tests. Once again the form of the variation in welds of two alloys is similar but with detail differences. Lowest crack growth rates are near the weld centreline, climb to a peak at 5mm in 7150 and 7-9 mm in 2024. Growth rates decline to a minimum at 8-10 mm in 7150 and 10 mm in 2024, before rising to a peak at 15 mm followed by a slow decline. Growth rates at the maxima and minima change by a factor of 12 in 7150 but a factor of 5 to 6 only in 2024.

DISCUSSION

MIG welds in both alloys produce complex profiles of residual stress and hardness. The peaks and troughs are not generally coincident, and interpretation of the constant ΔK growth rate behaviour is therefore made difficult. In 7150 welds, the peak hardness, largest residual stress, and fastest growth rate all occur at 5-6 mm from the weld centreline. Slow growth rates occur at both the centreline (a region of low hardness and moderate residual stress), and at a region 8-10 mm from the centreline; a region of low hardness and relatively large residual stress. This suggests that both local hardness and local residual stress have a role in determining local crack growth rates.

In 2024 welds, residual stresses are generally 20-25 MPa greater than in 7150. The peaks and troughs of growth rate at constant ΔK do not coincide with those of the hardness and residual stress profiles in the same way as for the 7150 welds. The lowest hardness is at the weld centreline, and this coincides with the smallest growth rates. However the peak in hardness is at the fusion zone/ HAZ boundary 3

mm from the weld centreline. The fastest growth rates are at 15 mm with a lesser peak at 7 to 8 mm. The 15 mm peak does coincide with the greatest residual stress.

This result conflicts with that found by Bussu and Irving [16,17] in friction stir welds of 2024-T351, in which residual stress was found to dominate fatigue crack growth rates. However, friction stir welds do not contain a fusion zone, and the local microstructure does not contain inhomogeneities and interdendritic shrinkage defects in a different composition alloy. It might be expected that microstructure and hardness would play less of a role in solid-state welds than in fusion ones.

For samples with thumbnail surface flaws, the crack will start growing in weld metal. When the surface crack tip reaches the high hardness and high tensile residual stress zone, the crack tip in the thickness direction will still remain in the softer and lower residual stress zone. On other hand, when the crack tip in the sample with a central through crack propagates into the high tensile residual stress zone, the majority of the crack front will be under the action of high hardness and high tensile residual stress. The results shown Figure 3(b), which shows the crack growth rate in weld metal of samples with through cracks was significantly faster than that in the part through crack. In support of this argument, 7150 welds exhibited the greatest difference in growth rate between surface and through cracks. Fatigue cracks for constant ΔK in 7150 welds showed the greatest changes in growth rate from weld centreline to the maximum at 6 mm distance. This will cause through cracks to grow faster.

CONCLUSIONS

(1) MIG welded 2024 and 7150 aluminium alloys contain complex tensile residual stress fields, hardness and microstructure variation. Local fatigue crack growth rates are sensitive to these changes.

(2) Fatigue crack growth behaviour under tensile mean stresses is influenced by tensile residual stress and hardness distribution, particularly in 7150 welds. This behaviour is unlike that of friction stir welds which are primarily influenced by residual stress only.

(3) Fatigue crack propagation behaviour under these conditions will be sensitive to crack shape and the growth path.

ACKNOWLEDGEMENTS

TABLE 1   Typical Transverse Tensile Test Results for MIG Welded Plates

Alloy	0.2% Proof Strenth (*MPa*)		Tensile Strength (*MPa*)		Elongation (%)	
	Parent	Welds	Parent	Welds	Parent	Welds
2024	320	313	460	388	14	3.3
7150	570	367	610	381	9	2.0
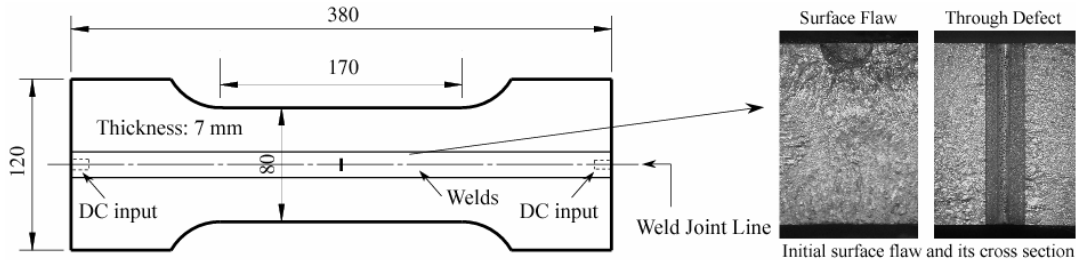
FIGURE 1. Geometry and dimensions of the Dog-bone coupon samples, and the cross section of thumbnail surface flaw

(a) MIG welded 2024

(b) MIG welded 7150
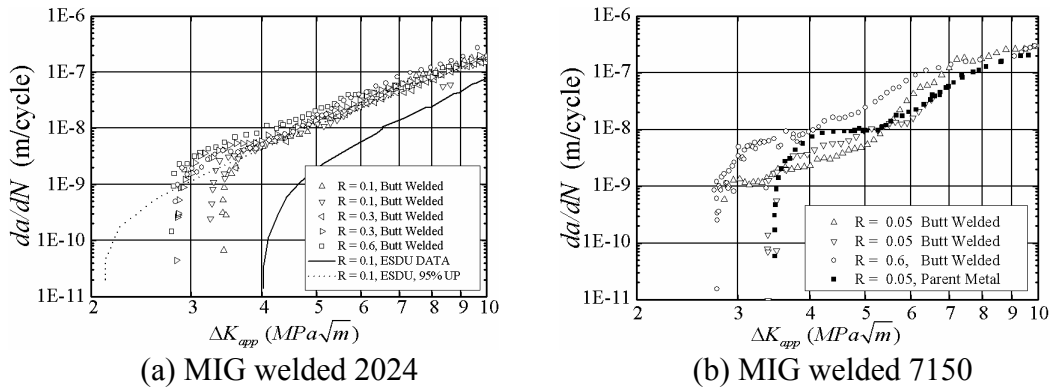
Figure 2. Results of constant amplitude load fatigue crack growth test on different R ratios for MIG welded aluminum alloys

(a) MIG welded 2024
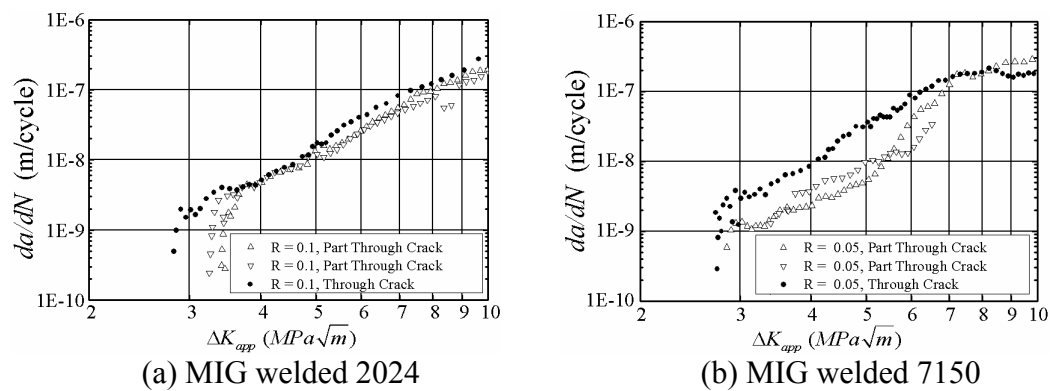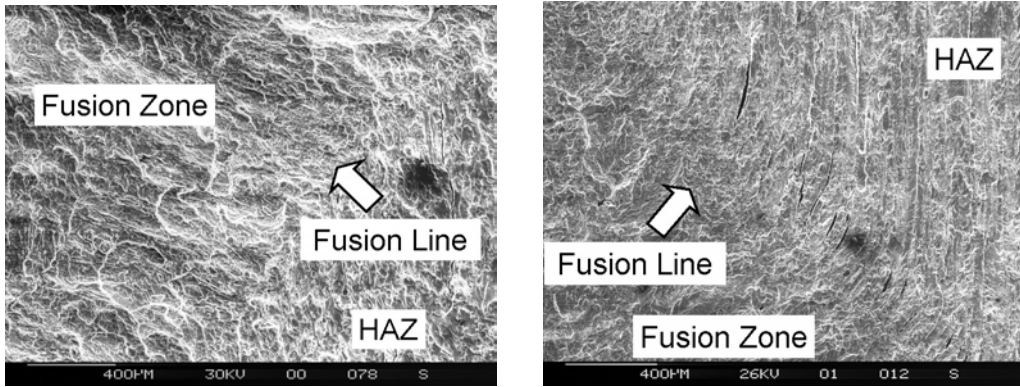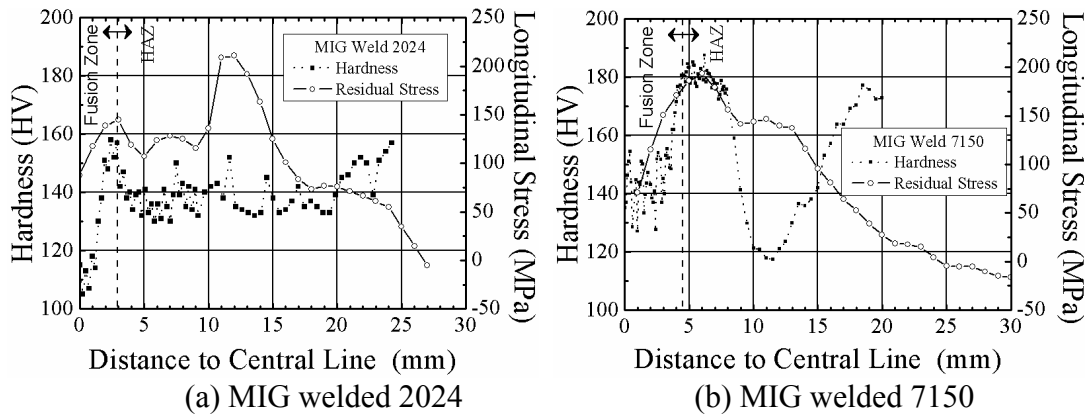

(b) MIG welded 7150

Figure 3. Comparison of constant amplitude load fatigue crack growth test results for MIG welded aluminum alloys coupon samples with different initial flaws.

(a) MIG welded 2024   (b) MIG welded 7150

Figure 4. Fractography in the boundary of fusion and HAZ of part through crack samples

(a) MIG welded 2024   (b) MIG welded 7150

Figure 5. Hardness profile and longitudinal residual stress distribution in the central line along the transverse direction of the welds cross-section.
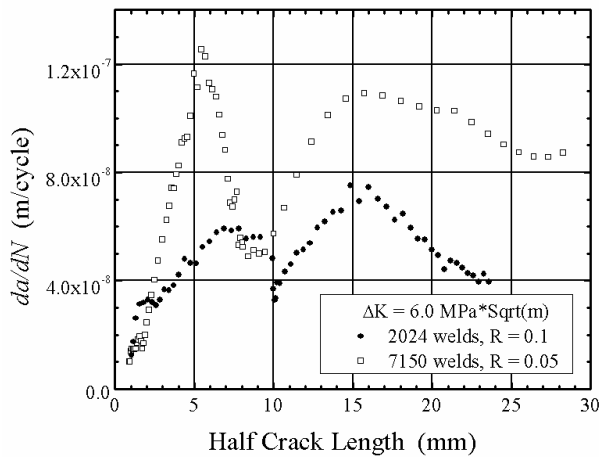

Figure 6. Constant ΔK fatigue crack growth test results for MIG welds

REFERENCE LIST

(1) Woodward, N.J., Thomas, A., Sci. Technol. Welding Joining, Vol. 5, No. 1, 2000, pp.21–25.

(2) Woodward N.J., et al., 7th International Conference: Joints in Aluminium, INALCO 98, Cambridge, UK, 1998.

(3) Thomas, W.M., 7th International Conference: Joints in Aluminium, INALCO 98, Cambridge, UK, 1998.

(4) Dawes, C.J., Thomas W.M., The Welding Journal, Vol. 75, No. 3, 1996, pp.41–46.

(5) Thomas, A.W., Phd. Thesis: Parameter Development for The MIG Welding of High Strength Aerospace Aluminium Alloys, Cranfield University, 2000.

(6) Schmidt, M. and Ohrloff, N., Structural Integrity for the next Millennium, Proceedings 20th Symposium ICAF, Edited by Rudd, J. L. and Bader, R.M., ICAF99, pp.537-552

(7) Jaccard, R., 7th International Conference on Joints in Aluminium, INALCO 2001, Munich Germany, 2001.

(8) El-Soudani S.M., Pelloux R.M., Welding J. Vol. 54, No. 5, 1979, pp.1445–1455.

(9) Tsay, L.W., Chern, T.S., Gau, CY, and Yang J.R., Int. J. Fatigue, Vol. 21, 1999, pp.857–864.

(10) Stelmukh, V., Edwards, L., Santisteban, J. R., Ganguly, S. and Fitzpatrick, M.E., Materials Science Forum 404-407, 2002, pp. 599-604.

(11) Stelmukh, V. and Edwards, L., Microscopy and Analysis, Vol. 90, pp. 15-18.

(12) Gangloff, R.P., Salavik, D.C., Piascik, R.S. and VanStone, R.H., Small-Crack Test Methods, Edited by J. M. Larsen and J. E. Allison, ASTM STP 1149, 1992, pp.116-168.

(13) VanStone, R.H. and Richardson, T.L., Automated Test Methods for Fracture and Fatigue Crack Growth. Edited by W. H. Cullen, R. W. Landgraf, L. R. Kaisand, and J. H. Underwood, ASTM STP 877, 1992, pp.148-166.

(14) Newman, J.C., and Raju, I.S., Computational Methods in the Mechannics of Fracture. Edited by S. N. Atluri, 1986, pp.312-350.

(15) Newman, J.C., and Raju, I.S., Fracture Mechanics: Fourteenth Symposium--Volume I: Theory and Analysis, Edited by J. C. Lewis and G. Sines, ASTM STP791, 1983, pp.I-238-265.

(16) Bussu, G. and Irving, P.E., Design for Durability in Digital Age, 2001, pp.331–350.

(17) Bussu, G. and Irving, P.E., Int. J. of Fatigue, Vol. 25, 2003, pp. 77–88.

⊥

☐